



Numerical simulation for Darcy–Forchheimer three-dimensional rotating flow of nanofluid with prescribed heat and mass flux conditions

Tasawar Hayat^{1,2} · Arsalan Aziz¹ · Taseer Muhammad³ · Ahmed Alsaedi²

Received: 7 August 2018 / Accepted: 16 October 2018 / Published online: 26 October 2018
© Akadémiai Kiadó, Budapest, Hungary 2018

Abstract

Darcy–Forchheimer three-dimensional rotating flow of nanofluid with prescribed heat and mass flux conditions is addressed. Flow is generated by an exponentially stretchable surface. Thermophoretic diffusion and random motion are employed. Suitable transformations lead to strong nonlinear ordinary differential system. An efficient numerical solver namely NDSolve is used to tackle the governing nonlinear system. Plots have been displayed in order to explore the role of flow parameters on the solutions. Moreover the skin-friction coefficients and heat and mass transfer rates are also plotted and discussed. It is noticed that the effects of porosity parameter and Forchheimer number on temperature field are quite similar. Both temperature and its associated thermal layer thickness are enhanced for larger porosity parameter and Forchheimer number.

Keywords 3D flow · Nanoparticles · Rotating frame · Darcy–Forchheimer porous space · Prescribed heat and mass flux conditions · Numerical solution

Introduction

Nanofluid is comparatively a newly recognized class of fluids containing carrier liquid with particles of nano-size. Basically some materials like oil, ethylene glycol, propylene glycol etc. in view of their weaker thermal conductivity have poor heat transfer properties. Thus, inclusion of nanoparticles in such type of carrier liquids is a quite charismatic way to enhance the thermal efficiency of such liquids. These nanoparticles are especially made of metals, oxide ceramics, carbide ceramics, non-metals and various other composite materials. Such nanoparticles have

distinctive physical and chemical features and have thermal efficiencies magnificently higher than carrier liquids. These nanoparticles are utilized in development and structural process of fiber production in textile, MHD power generators, petroleum reservoirs, cooling of nuclear reactors, cancer therapy, vehicle transformer, geothermal energy, safer surgery processes and many others. Recent inspections on nanofluid reveal that the carrier liquid has absolutely different features with the nanoparticle mixture because the thermal efficiency of carrier liquid is smaller than the nanoparticle's thermal efficiency. Appropriate storage of thermal energy and higher convective heat transfer coefficients are the main features of nanofluid. Nanofluids have various common applications in industrial and vehicle cooling, heat control systems, sensing, food industry, chemical industry, cooling towers, power production and efficiency of hybrid-powered engines etc. Initially, the idea of nanofluid was devised by Choi [1]. He concluded that the nanoparticles dramatically increase the thermal efficiency of carrier liquids. Buongiorno [2] developed the two-phase model of nanoparticles by considering the thermophoretic and Brownian motion aspects. Here we employed the Buongiorno model to study the

✉ Arsalan Aziz
arsalan_qau@yahoo.com

¹ Department of Mathematics, Quaid-I-Azam University, Islamabad 44000, Pakistan

² Nonlinear Analysis and Applied Mathematics (NAAM) Research Group, Department of Mathematics, Faculty of Science, King Abdulaziz University, Jeddah 21589, Saudi Arabia

³ Department of Mathematics, Government College Women University, Sialkot 51310, Pakistan

convective heat transfer characteristics in nanofluids. This model determined that the homogeneous-flow models are in conflict with the experimental results and tend to underpredict the heat transfer coefficient of nanofluid. While the dispersion effect is totally negligible as a result of nanoparticle size. Thus, Buongiorno proposed an alternative model that ignores the shortcomings of homogeneous and dispersion models. He affirmed that the abnormal heat transfer appears due to particle migration in the fluid. Exploring the nanoparticle migration, he considered the seven slip mechanisms that can produce a parallel velocity between the nanoparticles and base fluid. These are inertia, thermophoresis, Brownian diffusion, diffusiophoresis, Magnus effect, fluid drainage and gravity. He concluded that, of these seven, only Brownian diffusion and thermophoresis are important slip mechanisms in nanofluids. Based on such findings, he established a two-component four-equation nonhomogeneous equilibrium model for mass, momentum and heat transport in nanofluids. Tiwari and Das [3] also discussed the heat transfer experimentally of nanoliquids in a two-sided lid-driven heated square cavity. Pantzali et al. [4] discussed importance of CuO-water nanomaterials on the surface of heat exchangers experimentally. Review of thermal convective enhancement in nanofluids is reported by Kakac and Pramuanjaroenkij [5]. Abu-Nada and Oztop [6] explored effects of inclination angle in natural convective Cu-water nanofluid flow in enclosures. Few interesting studies about nanofluids can be seen via refs. [7–36].

The study of fluid flow and heat transport process in a porous media has achieved much attention of researchers due to its ample applications in technological, industrial, chemical and manufacturing processes. Such applications include crude oil production, nuclear-based repositories, casting and welding in manufacturing processes, nuclear waste disposal, units of the energy storage, fermentation processes and drying of a porous solid etc. The modification of classical Darcy's theory results in the non-Darcian porous space which involves inertial and boundary effects. The classical Darcy's law is applicable for a finite range of low velocity and smaller porosity. Forchheimer [37] considered inertia effects through the inclusion of a square velocity term in momentum equation. Muskat [38] entitled this contribution as Forchheimer factor. Mixed convective flow in a porous medium has been developed by Seddeek [39]. Jha and Kaurangini [40] presented approximate solutions for nonlinear Brinkman-Forchheimer-extended Darcy flow. Darcy-Forchheimer porous space in hydro-magnetic convective flow with non-uniform heat source/sink is studied by Pal and Mondal [41]. Darcy-Forchheimer flow of Maxwell material due to convectively heated sheet has been investigated by Sadiq and Hayat [42]. Shehzad et al. [43] employed Cattaneo-Christov heat

flux model for Darcy-Forchheimer flow of an Oldroyd-B fluid with variable conductivity and nonlinear convection. Forced convection stagnation-point flow with Darcy-Forchheimer expression is examined by Bakar et al. [44]. Hayat et al. [45] analyzed Darcy-Forchheimer flow with variable thermal conductivity and Cattaneo-Christov heat flux. A comparative study for Darcy-Forchheimer flow of viscoelastic nanofluids is studied by Hayat et al. [46]. Umavathi et al. [47] used Darcy-Forchheimer-Brinkman model in order to present a numerical study for natural convective flow of nanofluids. Darcy-Forchheimer flow of Maxwell nanofluid with convective boundary condition has been studied by Muhammad et al. [48]. Shekholeslami [49] discussed the impact of Lorentz forces on nanofluid flow in a porous cavity by means of non-Darcy model. A revised model for Darcy-Forchheimer three-dimensional flow of nanofluid subject to convective boundary condition is investigated by Muhammad et al. [50]. Darcy-Forchheimer three-dimensional flow of Williamson nanofluid induced by a convectively heated nonlinear stretching sheet is reported by Hayat et al. [51]. Recently Hayat et al. [52] present an optimal analysis for Darcy-Forchheimer 3D flow of Carreau nanofluid with convectively heated surface.

The investigators at present are engaged in analyzing the fluid flow and heat transport problem in rotating frame. It is because of their numerous applications in gas turbine rotors, rotating machinery, thermal power generation, electronic devices, aeronautics, air-cleaning machine and several others. Analytical solutions for viscous fluid flow over a stretched sheet in rotating frame are computed by Wang [53]. Takhar et al. [54] analyzed magnetohydrodynamics in rotating flow past a stretched sheet. Time-dependent rotating flow induced by an impulsively deforming surface is addressed by Nazar et al. [55]. Javed et al. [56] constructed local similar solutions for rotating flow induced by an exponentially deforming sheet. Zaimi et al. [57] investigated rotating flow of viscoelastic fluid by an impermeable stretchable sheet. Rosali et al. [58] numerically investigated rotating flow caused by an exponentially permeable sheet. Shafique et al. [59] studied simultaneous effects of activation energy and binary chemical reactions in rotating flow of Maxwell fluid. Mustafa et al. [60] discussed rotating flow of Maxwell fluid with variable thermal conductivity. Three-dimensional rotating flow of Maxwell nanoliquid is reported by Hayat et al. [61]. Darcy-Forchheimer three-dimensional rotating flow of water-based carbon nanotubes is explored by Hayat et al. [62]. Maqsood et al. [63] numerically investigated viscoelastic fluid flow subject to homogeneous-heterogeneous reactions in rotating frame. Mustafa et al. [64] computed analytical solutions of three-dimensional rotating flow of an Oldroyd-B liquid by considering Cattaneo-Christov theory.

Turkyilmazoglu [65] discussed the fluid flow and heat transfer over a rotating and vertically moving disk. Very recently Mustafa et al. [66] computed numerical solutions of rotating flow of nanofluid over an exponentially deforming sheet.

The prime interest in present study is to illustrate Darcy–Forchheimer three-dimensional flow of nanoliquid induced by an exponentially stretchable surface in rotating frame. Thermophoretic diffusion and random motion aspects are retained. Prescribed surface heat and mass fluxes are implemented at stretchable surface. The governing systems are solved numerically by NDSolve technique. Moreover temperature, concentration, surface drag coefficients and local Nusselt and Sherwood numbers are graphically illustrated.

Statement

Here we intend to illustrate steady 3D rotating flow of nanoliquid induced by an exponentially stretchable surface. Darcy–Forchheimer porous space is considered. Buongiorno model is implemented for nanoliquid transport process. Cartesian coordinate system is employed. The sheet stretches with velocity $u_w(x) = U_0 e^{x/L}$ where U_0 being positive constant. In addition fluid rotates about z -direction with constant angular velocity ω . The boundary layer expressions governing the three-dimensional (3D) rotating flow of viscous nanofluid in the absence of viscous dissipation and thermal radiation are [52, 66]:

$$\frac{\partial u}{\partial x} + \frac{\partial v}{\partial y} + \frac{\partial w}{\partial z} = 0, \tag{1}$$

$$u \frac{\partial u}{\partial x} + v \frac{\partial u}{\partial y} + w \frac{\partial u}{\partial z} - 2\omega v = v \frac{\partial^2 u}{\partial z^2} - \frac{v}{k^*} u - Fu^2, \tag{2}$$

$$u \frac{\partial v}{\partial x} + v \frac{\partial v}{\partial y} + w \frac{\partial v}{\partial z} + 2\omega u = v \frac{\partial^2 v}{\partial z^2} - \frac{v}{k^*} v - Fv^2, \tag{3}$$

$$u \frac{\partial T}{\partial x} + v \frac{\partial T}{\partial y} + w \frac{\partial T}{\partial z} = \alpha^* \frac{\partial^2 T}{\partial z^2} + \frac{(\rho c)_p}{(\rho c)_f} \left(D_B \left(\frac{\partial T}{\partial z} \frac{\partial C}{\partial z} \right) + \frac{D_T}{T_\infty} \left(\frac{\partial T}{\partial z} \right)^2 \right), \tag{4}$$

$$u \frac{\partial C}{\partial x} + v \frac{\partial C}{\partial y} + w \frac{\partial C}{\partial z} = D_B \left(\frac{\partial^2 C}{\partial z^2} \right) + \frac{D_T}{T_\infty} \left(\frac{\partial^2 T}{\partial z^2} \right). \tag{5}$$

Here one has the following conditions [23, 66]:

$$\left. \begin{aligned} u = u_w(x) = U_0 e^{x/L}, v = 0, w = 0, -k \left(\frac{\partial T}{\partial z} \right)_w = T_0 e^{\frac{(A+1)x}{2L}}, \\ -D_B \left(\frac{\partial C}{\partial z} \right)_w = C_0 e^{\frac{(B+1)x}{2L}} \text{ at } z = 0, \end{aligned} \right\} \tag{6}$$

$$u \rightarrow 0, v \rightarrow 0, T \rightarrow T_\infty, C \rightarrow C_\infty \text{ when } z \rightarrow \infty. \tag{7}$$

Note that u, v and w represent the velocity components in x -, y -, and z -directions while $\nu (= \mu/\rho_f)$, μ and ρ_f stands for kinematic viscosity, dynamic viscosity and density of base liquid, k^* for permeability of porous medium, $F = C_b/xk^{*1/2}$ for non-uniform inertia coefficient of porous space, C_b for drag coefficient, $\alpha^* = k/(\rho c)_f$, $k, (\rho c)_f$ and $(\rho c)_p$ for thermal diffusivity, thermal efficiency, heat capacity of liquid and effective heat capacity of nanomaterials, respectively, T for temperature, D_B for Brownian diffusivity, C for concentration, D_T for thermophoretic diffusion coefficient, U_0, T_0 and C_0 for positive constants, L for reference length, A, B, T_∞ and C_∞ for temperature exponent, concentration exponent, ambient fluid temperature and ambient fluid concentration, respectively. Considering

$$\left. \begin{aligned} u = U_0 e^{x/L} f'(\zeta), v = U_0 e^{x/L} g(\zeta), \\ w = -\left(\frac{\nu U_0}{2L} \right)^{1/2} e^{x/2L} (f(\zeta) + \zeta f'(\zeta)), \\ T = T_\infty + \frac{T_0}{k} \sqrt{\frac{2\nu L}{U_0}} e^{Ax/2L} \theta(\zeta), C = C_\infty + \frac{C_0}{D_B} \sqrt{\frac{2\nu L}{U_0}} e^{Bx/2L} \varphi(\zeta), \\ \zeta = \left(\frac{U_0}{2\nu L} \right)^{1/2} e^{x/2L} z, \end{aligned} \right\} \tag{8}$$

Equation (1) is identically verified while Eqs. (2)–(7) yield

$$f''' + ff'' - 2f'^2 + 4\Omega g - 2\lambda f' - 2Fr f'^2 = 0, \tag{9}$$

$$g'' + fg' - 2f'g - 4\Omega f' - 2\lambda g - 2Fr g^2 = 0, \tag{10}$$

$$\theta'' + Pr (f\theta' - Af'\theta + N_b \theta' \varphi' + N_t \theta'^2) = 0, \tag{11}$$

$$\varphi'' + Sc (f\varphi' - Bf'\varphi) + \frac{N_t}{N_b} \theta'' = 0, \tag{12}$$

$$f(0) = g(0) = 0, f'(0) = 1, \theta'(0) = -1, \varphi'(0) = -1, \tag{13}$$

$$f'(\infty) \rightarrow 0, g(\infty) \rightarrow 0, \theta(\infty) \rightarrow 0, \varphi(\infty) \rightarrow 0. \tag{14}$$

Here rotation parameter, porosity parameter, Forchheimer number, Prandtl number, thermophoresis parameter, Schmidt number and Brownian motion parameter are symbolized by $\Omega, \lambda, Fr, Pr, N_t, Sc$ and N_b , respectively. Nondimensional forms of these parameters are given below:

$$\left. \begin{aligned} \lambda &= \frac{\nu L}{k' u_w}, Fr = \frac{C_b}{k'^{1/2}}, \Omega = \frac{\omega L}{u_w}, Pr = \frac{\nu}{\alpha^*}, Sc = \frac{\nu}{D_b}, \\ N_b &= \frac{(\rho c)_p D_b (C_w - C_\infty)}{(\rho c)_f \nu}, N_t = \frac{(\rho c)_p D_T (T_w - T_\infty)}{(\rho c)_f \nu T_\infty} \end{aligned} \right\} \quad (15)$$

The nondimensional forms of coefficients of skin friction and local Nusselt and Sherwood numbers are

$$\left. \begin{aligned} \left(\frac{Re_x}{2}\right)^{1/2} C_{fx} &= f''(0), \\ \left(\frac{Re_x}{2}\right)^{1/2} C_{fy} &= g'(0), \\ \frac{L}{x} \left(\frac{Re_x}{2}\right)^{-1/2} Nu_x &= \frac{1}{\theta(0)}, \\ \frac{L}{x} \left(\frac{Re_x}{2}\right)^{-1/2} Sh_x &= \frac{1}{\phi(0)}. \end{aligned} \right\} \quad (16)$$

In above expressions $Re_x = u_w x / \nu$ represents the local Reynolds number.

Discussion

This section addresses the contributions of local porosity parameter λ , Brownian motion parameter N_b , Forchheimer number Fr , Schmidt number Sc , temperature exponent A , local rotational parameter Ω , Prandtl number Pr , thermophoresis parameter N_t and concentration exponent B on nondimensional temperature $\theta(\zeta)$ and concentration $\phi(\zeta)$ fields. Figure 1 displays variation of temperature field $\theta(\zeta)$ for various local porosity parameter λ . An increment in porosity parameter λ causes stronger temperature field $\theta(\zeta)$ and related layer thickness. Physically existence of porous space generates resistance in fluid motion and ultimate it decays in velocity of fluid. Hence an increment is noticed for temperature $\theta(\zeta)$ and associated thermal layer thickness. Figure 2 is plotted to explore impact of Forchheimer number Fr on temperature field $\theta(\zeta)$. Larger Fr correspond to increasing trend in temperature field $\theta(\zeta)$. Figure 3 presents influence of Ω on temperature field $\theta(\zeta)$. Higher local rotational parameter Ω enhance temperature field $\theta(\zeta)$ and associated layer thickness. Figure 4 elucidates that temperature field $\theta(\zeta)$ shows decreasing trend for higher values of temperature exponent A . Figure 5 shows

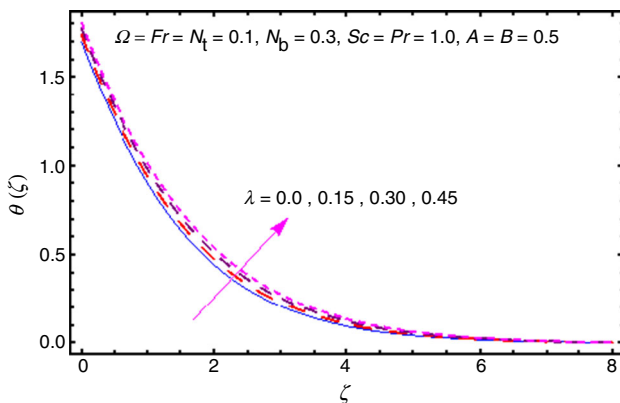


Fig. 1 $\theta(\zeta)$ variation for λ

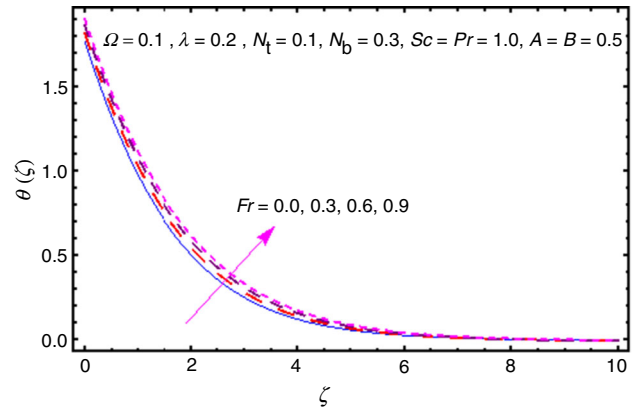


Fig. 2 $\theta(\zeta)$ variation for Fr

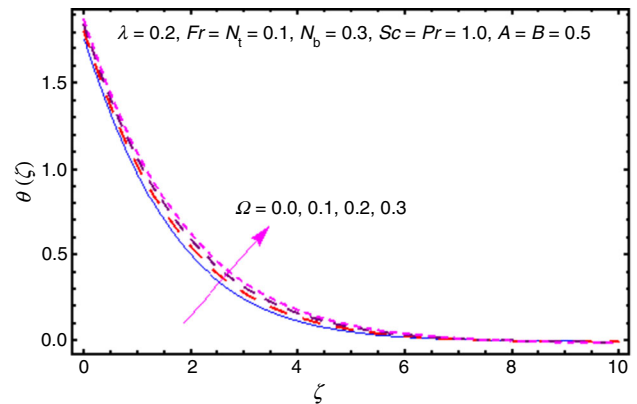


Fig. 3 $\theta(\zeta)$ variation for Ω

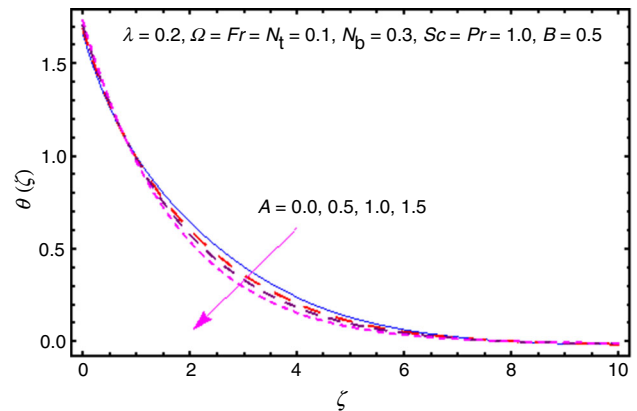


Fig. 4 $\theta(\zeta)$ variation for A

temperature field $\theta(\zeta)$ for varying Prandtl number Pr . Temperature field $\theta(\zeta)$ decayed for higher Pr . Figure 6 is sketched to examine that how temperature field $\theta(\zeta)$ gets affected with the variation of Brownian motion parameter N_b . By increasing N_b , the temperature field $\theta(\zeta)$ shows increasing trend. Physically the random motion of nanoparticles enhances by increasing Brownian motion parameter N_b due to which collision of particles occurs. As

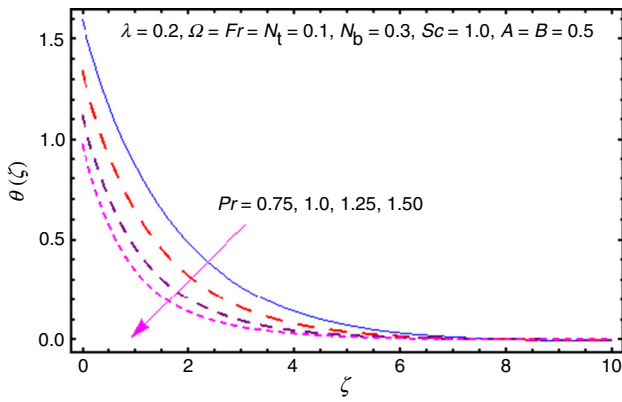


Fig. 5 $\theta(\zeta)$ variation for Pr

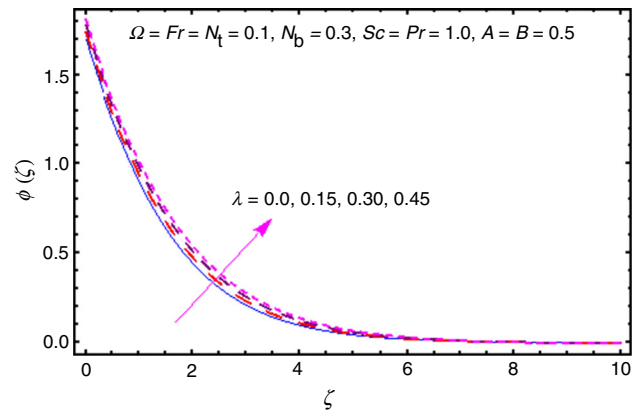


Fig. 8 $\phi(\zeta)$ variation for λ

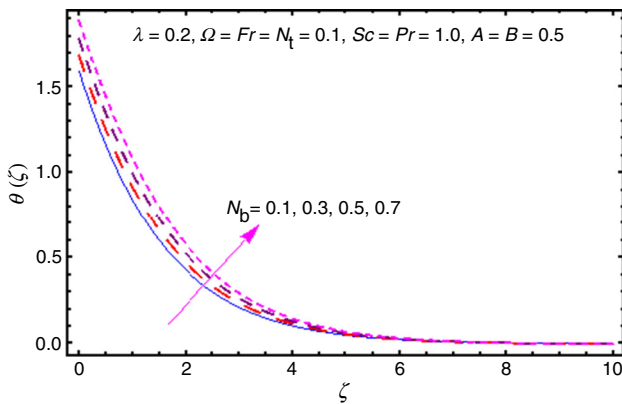


Fig. 6 $\theta(\zeta)$ variation for N_b

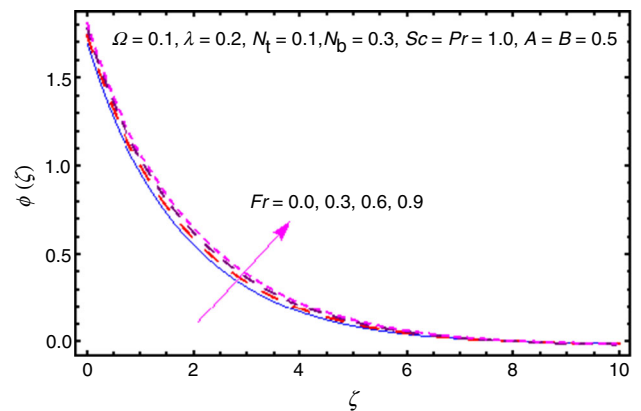


Fig. 9 $\phi(\zeta)$ variation for Fr

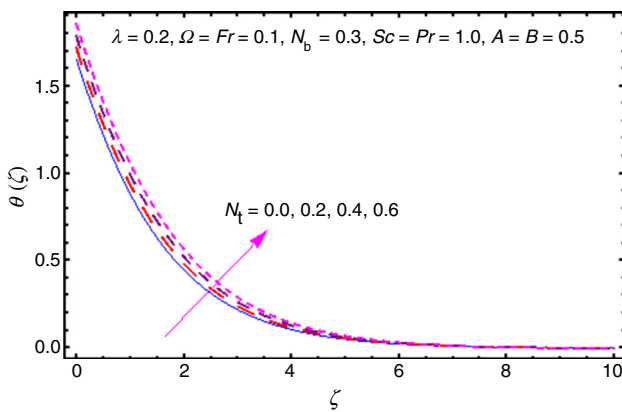


Fig. 7 $\theta(\zeta)$ variation for N_t

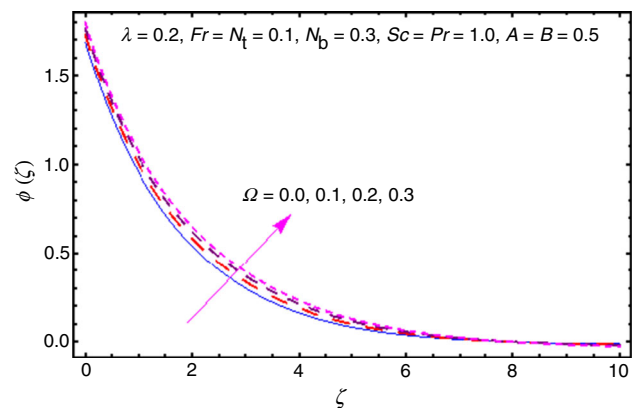


Fig. 10 $\phi(\zeta)$ variation for Ω

a result kinetic energy is converted into heat energy which causes an enhancement in temperature and related layer thickness. Figure 7 elaborates the influence of thermophoresis parameter N_t on temperature $\theta(\zeta)$. Clearly, temperature field is enhanced via larger N_t . Figure 8 illustrates that concentration field $\phi(\zeta)$ shows increasing trend via local porosity parameter λ . From Fig. 9 it is noted that Forchheimer number Fr yields higher concentration

field $\phi(\zeta)$. Figure 10 elaborates that how the concentration field $\phi(\zeta)$ is affected by higher values of local rotational parameter Ω . Here both temperature field and related layer thickness are elevated by increasing Ω . Figure 11 illustrates the variation in concentration field $\phi(\zeta)$ for concentration exponent C . Larger concentration exponent yields lower concentration field $\phi(\zeta)$ and related layer thickness. Effect of Schmidt number Sc on $\phi(\zeta)$ is sketched

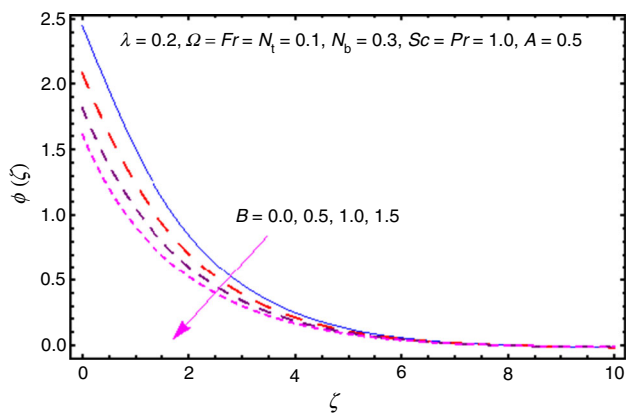


Fig. 11 $\phi(\zeta)$ variation for B

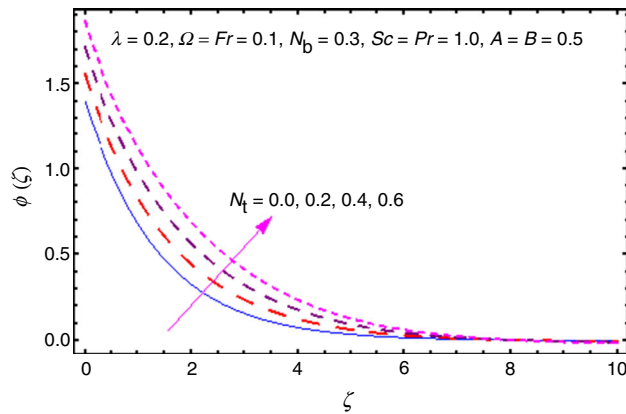


Fig. 14 $\phi(\zeta)$ variation for N_t

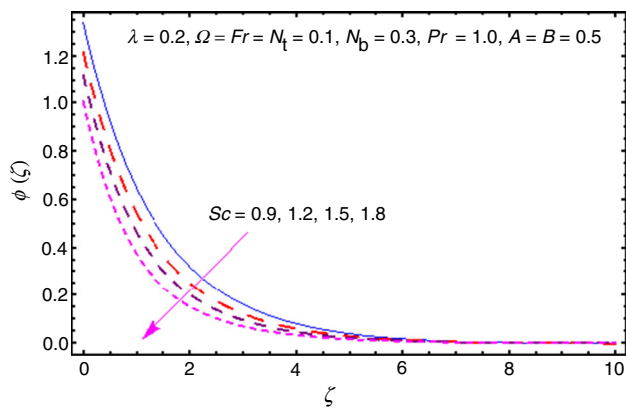


Fig. 12 $\phi(\zeta)$ variation for Sc

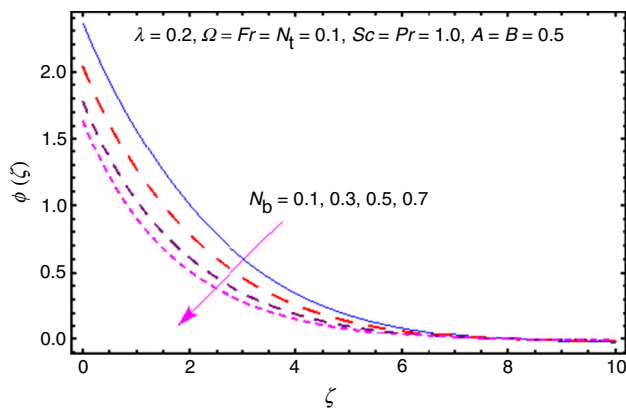


Fig. 13 $\phi(\zeta)$ variation for N_b

in Fig. 12. Here concentration field $\phi(\zeta)$ exhibits decreasing trend via larger Schmidt number Sc . Figure 13 is portrayed to deliberate the variation in concentration field under the influence of Brownian motion parameter N_b . An increment in N_b causes a decay in concentration. Here an enhancement in thermophoresis means that the nanoparticles are migrated from warm zone to cold zone. Therefore higher number of nanoparticles is dragged away

Table 1 Numerical data of surface drag coefficients $-f''(0)$ and $-g'(0)$ for distinct estimations of λ , Fr and Ω

λ	Fr	Ω	$-f''(0)$	$-g'(0)$
0.0	0.1	0.1	1.351292	0.197898
0.1			1.420528	0.179629
0.2			1.487723	0.165819
0.2	0.1	0.1	1.487723	0.165819
	0.2		1.531017	0.164732
	0.3		1.573174	0.163694
0.2	0.1	0.05	1.479441	0.083713
		0.1	1.487723	0.165819
		0.2	1.517052	0.320662

from the warm zone due to which nanoliquid concentration decays. Figure 14 presents the outcome of thermophoresis parameter N_t for concentration field $\phi(\zeta)$. Larger thermophoresis parameter N_t give an enhancement in $\phi(\zeta)$ and related layer thickness. Table 1 is calculated in order to investigate the numerical computations of skin-friction coefficients $-f''(0)$ and $-g'(0)$ for several estimations of porosity parameter λ , Forchheimer number Fr and rotation parameter Ω . Surface drag coefficients are increasing functions of Ω while reverse behavior is noticed for larger λ and Fr . Table 2 shows the numerical computations of local Nusselt number $\frac{1}{\theta(0)}$ and local Sherwood number $\frac{1}{\phi(0)}$ for different values of λ , Fr , Ω , Sc , Pr , N_t and N_b when $A = B = 0.5$. Heat transfer rate (local Nusselt number) decays via λ , Fr , Ω , N_t and N_b . Effects of Sc and Pr on heat transfer rate are quite similar. It is also observed that mass transfer rate (local Sherwood number) has lower and higher values for larger (λ , Fr , Ω , Pr , N_t , N_b) and (Sc), respectively.

Table 2 Numerical computations of local Nusselt number $\frac{1}{\theta(0)}$ and local Sherwood number $\frac{1}{\phi(0)}$ for various values of λ , Fr , Ω , N_t , Sc , N_b and Pr when $A = B = 0.5$.

λ	Fr	Ω	N_t	Sc	N_b	Pr	$\frac{1}{\theta(0)}$	$\frac{1}{\phi(0)}$
0.0	0.1	0.1	0.1	1.0	0.3	1.0	0.588588	0.611136
							0.574766	0.597735
							0.560822	0.584156
0.2	0.1	0.1	0.1	1.0	0.3	1.0	0.560822	0.584156
							0.555576	0.579322
							0.550526	0.564681
0.2	0.1	0.0	0.1	1.0	0.3	1.0	0.567862	0.591813
							0.560822	0.584156
							0.542852	0.565183
0.2	0.1	0.1	0.1	1.0	0.3	1.0	0.560822	0.584156
							0.190363	0.294592
							0.013188	0.013188
0.2	0.1	0.1	0.1	0.5	0.3	1.0	0.540982	0.350973
							0.560822	0.584156
							0.572558	0.785375
0.2	0.1	0.1	0.1	1.0	0.1	1.0	0.628977	0.584156
							0.593994	0.533559
							0.560822	0.423571
0.2	0.1	0.1	0.1	1.0	0.3	0.7	0.454659	0.588643
							1.0	0.560822
							1.3	0.648453

Conclusions

Darcy–Forchheimer three-dimensional (3D) rotating flow of nanoliquid due to stretchable surface with constant heat and mass flux conditions is discussed. The prime findings of present study have been structured as follows:

- Higher porosity parameter λ and Forchheimer number Fr exhibit similar trend for both temperature $\theta(\zeta)$ and concentration $\phi(\zeta)$ fields.
- Both temperature $\theta(\zeta)$ and concentration $\phi(\zeta)$ fields represent increasing behavior for higher local rotational parameter Ω .
- An increment in temperature exponent A and concentration exponent B leads to reduce temperature $\theta(\zeta)$ and concentration $\phi(\zeta)$ fields.
- Larger Prandtl Pr and Schmidt Sc numbers correspond to lower temperature and concentration fields.
- Brownian motion parameter N_b for temperature and concentration has reverse effects.
- Both temperature and concentration profiles are increased via thermophoresis parameter N_t .

References

1. Choi SUS. Enhancing thermal conductivity of fluids with nanoparticles. In: USA, ASME, FED 231/MD, vol 66. 1995; PP. 99–105.
2. Buongiorno J. Convective transport in nanofluids. J Heat Transf. 2006;128:240–50.
3. Tiwari RK, Das MK. Heat transfer augmentation in a two-sided lid-driven differentially heated square cavity utilizing nanofluid. Int J Heat Mass Transf. 2007;50:2002–18.
4. Pantzali MN, Mouza AA, Paras SV. Investigating the efficacy of nanofluids as coolants in plate heat exchangers (PHE). Chem Eng Sci. 2009;64:3290–300.
5. Kakac S, Pramuanjaroenkij A. Review of convective heat transfer enhancement with nanofluids. Int J Heat Mass Transf. 2009;52:3187–96.
6. Abu-Nada E, Oztop HF. Effects of inclination angle on natural convection in enclosures filled with Cu-water nanofluid. Int J Heat Fluid Flow. 2009;30:669–78.
7. Mustafa M, Hayat T, Pop I, Asghar S, Obaidat S. Stagnation-point flow of a nanofluid towards a stretching sheet. Int J Heat Mass Transf. 2011;54:5588–94.
8. Turkiylmazoglu M. Exact analytical solutions for heat and mass transfer of MHD slip flow in nanofluids. Chem Eng Sci. 2012;84:182–7.
9. Hsiao KL. Nanofluid flow with multimedia physical features for conjugate mixed convection and radiation. Comput Fluids. 2014;104:1–8.
10. Hayat T, Aziz A, Muhammad T, Ahmad B. Influence of magnetic field in three-dimensional flow of couple stress nanofluid over a nonlinearly stretching surface with convective condition. PLoS ONE. 2015;10:e0145332.
11. Ellahi R, Hassan M, Zeeshan A. Shape effects of nanosize particles in Cu-H₂O nanofluid on entropy generation. Int J Heat Mass Transf. 2015;81:449–56.
12. Hayat T, Muhammad T, Alsaedi A, Alhuthali MS. Magnetohydrodynamic three-dimensional flow of viscoelastic nanofluid in the presence of nonlinear thermal radiation. J Magn Magn Mater. 2015;396:31–7.
13. Chamkha A, Abbasbandy S, Rashad AM. Non-Darcy natural convection flow for non-Newtonian nanofluid over cone saturated in porous medium with uniform heat and volume fraction fluxes. Int. J. Numer. Methods Heat Fluid Flow. 2015;25:422–37.
14. Hayat T, Aziz A, Muhammad T, Alsaedi A. On magnetohydrodynamic three-dimensional flow of nanofluid over a convectively heated nonlinear stretching surface. Int J Heat Mass Transf. 2016;100:566–72.
15. Goshayeshi HR, Safaei MR, Goodarzi M, Dahari M. Particle size and type effects on heat transfer enhancement of Ferro-nanofluids in a pulsating heat pipe. Powder Technol. 2016;301:1218–26.
16. Shehzad N, Zeeshan A, Ellahi R, Vafai K. Convective heat transfer of nanofluid in a wavy channel: Buongiorno’s mathematical model. J Mol Liq. 2016;222:446–55.
17. Hayat T, Aziz A, Muhammad T, Alsaedi A. Numerical study for nanofluid flow due to a nonlinear curved stretching surface with convective heat and mass conditions. Results Phys. 2017;7:3100–6.
18. Eid MR, Alsaedi A, Muhammad T, Hayat T. Comprehensive analysis of heat transfer of gold-blood nanofluid (Sisko-model) with thermal radiation. Results Phys. 2017;7:4388–93.
19. Hayat T, Aziz A, Muhammad T, Alsaedi A. Active and passive controls of Jeffrey nanofluid flow over a nonlinear stretching surface. Results Phys. 2017;7:4071–8.
20. Waqas M, Khan MI, Hayat T, Alsaedi A. Numerical simulation for magneto Carreau nanofluid model with thermal radiation: a

- revised model. *Comput Methods Appl Mech Eng.* 2017;324:640–53.
21. Hayat T, Aziz A, Muhammad T, Alsaedi A. A revised model for Jeffrey nanofluid subject to convective condition and heat generation/absorption. *PLoS ONE.* 2017;12:e0172518.
 22. Sheikholeslami M, Hayat T, Alsaedi A. Numerical simulation of nanofluid forced convection heat transfer improvement in existence of magnetic field using lattice Boltzmann method. *Int J Heat Mass Transf.* 2017;108:1870–83.
 23. Hayat T, Aziz A, Muhammad T, Alsaedi A. Three-dimensional flow of nanofluid with heat and mass flux boundary conditions. *Chin J Phys.* 2017;55:1495–510.
 24. Mahanthesh B, Gireesha BJ, Kumara BCP, Shashikumar NS. Marangoni convection radiative flow of dusty nanoliquid with exponential space dependent heat source. *Phys E: Low Dimens Syst. Nanostruct.* 2017;94:25–30.
 25. Mahanthesh B, Kumar PBS, Gireesha BJ, Manjunatha S, Gorla RSR. Nonlinear convective and radiated flow of Tangent Hyperbolic liquid due to stretched surface with convective condition. *Results Phys.* 2017;7:2404–10.
 26. Mahanthesh B, Gireesha BJ. Scrutinization of thermal radiation, viscous dissipation and Joule heating effects on Marangoni convective two-phase flow of Casson fluid with fluid-particle suspension. *Results Phys.* 2018;8:869–78.
 27. Mahanthesh B, Gireesha BJ, Shehzad SA, Rauf A, Kumar PBS. Nonlinear radiated MHD flow of nanoliquids due to a rotating disk with irregular heat source and heat flux condition. *Phys B.* 2018;537:98–104.
 28. Mahanthesh B, Gireesha BJ, Sheikholeslami M, Shehzad SA, Kumar PBS. Nonlinear radiative flow of Casson nanoliquid past a cone and wedge with magnetic dipole: mathematical model of renewable energy. *J Nanofluids.* 2018;7:1089–100.
 29. Gireesha BJ, Kumar PBS, Mahanthesh B, Shehzad SA, Abbasi FM. Nonlinear gravitational and radiation aspects in nanoliquid with exponential space dependent heat source and variable viscosity. *Microgravity Sci Technol.* 2018;30:257–64.
 30. Rashidi S, Eskandarian M, Mahian O, Poncet S. Combination of nanofluid and inserts for heat transfer enhancement. *J Therm Anal Calorim.* 2018. <https://doi.org/10.1007/s10973-018-7070-9>.
 31. Rashidi S, Mahian O, Languri EM. Applications of nanofluids in condensing and evaporating systems. *J Therm Anal Calorim.* 2018;131:2027–39.
 32. Akar S, Rashidi S, Esfahani JA. Second law of thermodynamic analysis for nanofluid turbulent flow around a rotating cylinder. *J Therm Anal Calorim.* 2018;132:1189–200.
 33. Animasaun IL, Koriko OK, Adegbe KS, Babatunde HA, Ibraheem RO, Sandeep N, Mahanthesh B. Comparative analysis between 36 nm and 47 nm alumina-water nanofluid flows in the presence of Hall effect. *J Therm Anal Calorim.* 2018. <https://doi.org/10.1007/s10973-018-7379-4>.
 34. Ullah I, Waqas M, Hayat T, Alsaedi A, Khan MI. Thermally radiated squeezed flow of magneto-nanofluid between two parallel disks with chemical reaction. *J Therm Anal Calorim.* 2018. <https://doi.org/10.1007/s10973-018-7482-6>.
 35. Turkyilmazoglu M. Analytical solutions to mixed convection MHD fluid flow induced by a nonlinearly deforming permeable surface. *Commun Nonlinear Sci Numer Simul.* 2018;63:373–9.
 36. Turkyilmazoglu M. Buongiorno model in a nanofluid filled asymmetric channel fulfilling zero net particle flux at the walls. *Int J Heat Mass Transf.* 2018;126:974–9.
 37. Forchheimer P. Wasserbewegung durch boden. *Z Ver D Ing.* 1901;45:1782–8.
 38. Muskat M. The flow of homogeneous fluids through porous media. Edwards, MI; 1946.
 39. Seddeek MA. Influence of viscous dissipation and thermophoresis on Darcy–Forchheimer mixed convection in a fluid saturated porous media. *J Colloid Interface Sci.* 2006;293:137–42.
 40. Jha BK, Kaurangini ML. Approximate analytical solutions for the nonlinear Brinkman–Forchheimer-extended Darcy flow model. *Appl Math.* 2011;2:1432–6.
 41. Pal D, Mondal H. Hydromagnetic convective diffusion of species in Darcy–Forchheimer porous medium with non-uniform heat source/sink and variable viscosity. *Int Commun Heat Mass Transf.* 2012;39:913–7.
 42. Sadiq MA, Hayat T. Darcy–Forchheimer flow of magneto Maxwell liquid bounded by convectively heated sheet. *Results Phys.* 2016;6:884–90.
 43. Shehzad SA, Abbasi FM, Hayat T, Alsaedi A. Cattaneo–Christov heat flux model for Darcy–Forchheimer flow of an Oldroyd-B fluid with variable conductivity and non-linear convection. *J Mol Liq.* 2016;224:274–8.
 44. Bakar SA, Arifin NM, Nazar R, Ali FM, Pop I. Forced convection boundary layer stagnation-point flow in Darcy–Forchheimer porous medium past a shrinking sheet. *Front Heat Mass Transf.* 2016;7:38.
 45. Hayat T, Muhammad T, Al-Mezal S, Liao SJ. Darcy–Forchheimer flow with variable thermal conductivity and Cattaneo–Christov heat flux. *Int J Numer Methods Heat Fluid Flow.* 2016;26:2355–69.
 46. Hayat T, Haider F, Muhammad T, Alsaedi A. On Darcy–Forchheimer flow of viscoelastic nanofluids: a comparative study. *J Mol Liq.* 2017;233:278–87.
 47. Umavathi JC, Ojjela O, Vajravelu K. Numerical analysis of natural convective flow and heat transfer of nanofluids in a vertical rectangular duct using Darcy–Forchheimer–Brinkman model. *Int J Therm Sci.* 2017;111:511–24.
 48. Muhammad T, Alsaedi A, Shehzad SA, Hayat T. A revised model for Darcy–Forchheimer flow of Maxwell nanofluid subject to convective boundary condition. *Chin J Phys.* 2017;55:963–76.
 49. Sheikholeslami M. Influence of Lorentz forces on nanofluid flow in a porous cavity by means of non-Darcy model. *Eng Comput.* 2017;34:2651–67.
 50. Muhammad T, Alsaedi A, Hayat T, Shehzad SA. A revised model for Darcy–Forchheimer three-dimensional flow of nanofluid subject to convective boundary condition. *Results Phys.* 2017;7:2791–7.
 51. Hayat T, Aziz A, Muhammad T, Alsaedi A. Darcy–Forchheimer three-dimensional flow of Williamson nanofluid over a convectively heated nonlinear stretching surface. *Commun Theor Phys.* 2017;68:387–94.
 52. Hayat T, Aziz A, Muhammad T, Alsaedi A. An optimal analysis for Darcy–Forchheimer 3D flow of Carreau nanofluid with convectively heated surface. *Results Phys.* 2018;9:598–608.
 53. Wang CY. Stretching a surface in a rotating fluid. *Z Angew Math Phys.* 1988;39:177–85.
 54. Takhar HS, Chamkha AJ, Nath G. Flow and heat transfer on a stretching surface in a rotating fluid with a magnetic field. *Int J Therm Sci.* 2003;42:23–31.
 55. Nazar R, Amin N, Pop I. Unsteady boundary layer flow due to a stretching surface in a rotating fluid. *Mech Res Commun.* 2004;31:121–8.
 56. Javed T, Sajid M, Abbas Z, Ali N. Non-similar solution for rotating flow over an exponentially stretching surface. *Int J Numer Methods Heat Fluid Flow.* 2011;21:903–8.
 57. Zaimi K, Ishak A, Pop I. Stretching surface in rotating viscoelastic fluid. *Appl Math Mech Engl Ed.* 2013;34:945–52.
 58. Rosali H, Ishak A, Nazar R, Pop I. Rotating flow over an exponentially shrinking sheet with suction. *J Mol Liq.* 2015;211:965–9.

59. Shafique Z, Mustafa M, Mushtaq A. Boundary layer flow of Maxwell fluid in rotating frame with binary chemical reaction and activation energy. *Results Phys.* 2016;6:627–33.
60. Mustafa M, Hayat T, Alsaedi A. Rotating flow of Maxwell fluid with variable thermal conductivity: an application to non-Fourier heat flux theory. *Int J Heat Mass Transf.* 2017;106:142–8.
61. Hayat T, Muhammad T, Mustafa M, Alsaedi A. An optimal study for three dimensional flow of Maxwell nanofluid subject to rotating frame. *J Mol Liq.* 2017;229:541–7.
62. Hayat T, Haider F, Muhammad T, Alsaedi A. Three-dimensional rotating flow of carbon nanotubes with Darcy–Forchheimer porous medium. *PLoS ONE.* 2017;12:e0179576.
63. Maqsood N, Mustafa M, Khan JA. Numerical tackling for viscoelastic fluid flow in rotating frame considering homogeneous-heterogeneous reactions. *Results Phys.* 2017;7:3475–81.
64. Mustafa M, Hayat T, Alsaedi A. Rotating flow of Oldroyd-B fluid over stretchable surface with Cattaneo–Christov heat flux: analytic solutions. *Int J Numer Meth Heat Fluid Flow.* 2017;27:2207–22.
65. Turkyilmazoglu M. Fluid flow and heat transfer over a rotating and vertically moving disk. *Phys Fluids.* 2018;30:063605.
66. Mustafa M, Wasim M, Hayat T, Alsaedi A. A revised model to study the rotating flow of nanofluid over an exponentially deforming sheet: numerical solutions. *J Mol Liq.* 2017;225:320–7.